X-ray timing and spectral analysis of the propeller driven pulsar-like white dwarf AE Aquarii

B Oruru and P J Meintjes

Department of Physics, University of the Free State, P. O. Box 339, Bloemfontein 9300, ZA

E-mail: OruruB@ufs.ac.za, MeintjPJ@ufs.ac.za

Abstract. The highly transient multi-wavelength system AE Aqr is an ideal laboratory to study accretion and related astrophysical fluid dynamics. The system is in a propeller state, and the turbulent interaction between the fast spinning WD magnetosphere and the accretion flow is believed to play a crucial role in the characteristic multi-wavelength emission of the system. We have analysed the system's X-ray lightcurves and spectra from data observed with Chandra and Swift-XRT, and the results of this study show that the X-ray characteristics display a mixed signature of thermal and non-thermal emission. The luminosity of the observed hard X-rays is three orders of magnitudes less than the spin-down power of the white dwarf, which tends to correlate with rotation-driven pulsars. In this paper, the results of the analysis will be discussed, with the aim to propose suitable models for the X-ray emission mechanisms.

1. Introduction

AE Aquarii (AE Aqr) consists of a fast rotating magnetized white dwarf accreting matter from a late-type K3-5 main sequence companion (e.g. Patterson 1979; Welsh *et al* 1995; Itoh *et al* 2006). The binary companions are in orbit with a period of 9.88 h (e.g. Welsh *et al* 1993). Although an accretion disc is expected, the observed properties of the system do not conform to this. Wynn *et al* (1997) have proposed that the system is in a propeller phase, where the bulk of the mass flow is expelled from the system by the fast rotating magnetosphere of the white dwarf. However, plasma instabilities may attach some gaseous material onto the field lines which will then be accreted on the magnetic polar caps.

AE Aqr has been detected in almost all wavelength bands (e.g. de Jager 1991), from radio, through optical to TeV γ-rays (e.g. Bookbinder & Lamb 1987; Patterson 1979; Meintjes *et al* 1994). Patterson (1979) observed a 33 s coherent oscillation in the optical light, which were later observed in other wavelengths (e.g. Patterson *et al* 1980; de Jager *et al* 1994; Eracleous *et al* 1994). AE Aqr is a relatively bright X-ray source, and coupled with its close proximity to the earth, it has been observed regularly (e.g. Patterson *et al* 1980; Osborne 1989; Reinsch *et al* 1995; Itoh *et al* 2006). This paper will focus on the X-ray characteristics of the system based on the analysis of data from recent observations with Chandra and Swift.

2. Observations of AE Aquarii

The Chandra X-ray Satellite (e.g. Brissenden 2001) observed AE Aquarii on August 30, 2005 at 06:37 UT for $\sim$ 80 ks (ObsID 5431; e.g. Mauche 2006), using the Advanced CCD Imaging Spectrometer (ACIS-S) detector and the High Energy Transmission Grating (HETG). Standard

data processing was done at the Chandra X-ray Center (CXC), and data was acquired through the High Energy Astrophysics Science Archive Research Center (HEASARC) on-line service, provided by the NASA's Goddard Space Flight Center (GSFC). Data reduction and analysis were done using the Chandra Interactive Analysis of Observations (CIAO) software.

The Swift GRB explorer (e.g. Gehrels *et al* 2004) observed AE Aquarii (target ID = 30295) between August 30 and September 2, 2005 for a total duration of $\sim$ 10.5 ks, as a pre-planned target (PPT; e.g. Evans *et al* 2009). Data were archived in September 2005, and standard processing was done later at the UK Swift Science Data Centre (UKSSDC). The results presented in this paper are based on data collected when the XRT was operating in the PC mode, in which full imaging and spectroscopic resolutions are retained, but timing resolution is limited to 2.5 s (e.g. Burrows *et al* 2005). The lightcurve and spectral data files were obtained using the on-demand software (developed by the Swift team) through the HEASARC on-line service, provided by NASA's GSFC. The general discussion on the software usage are presented in the original papers by Evans *et al* (2007) and Evans *et al* (2009).

3. Results

3.1. Lightcurves

Figure 1 shows the background subtracted lightcurve from Chandra data. The source is highly variable, and exhibit flares. Flares with similar characteristics repeat after $\sim$ 10 hr, which corresponds to the orbital period of the system. The hardness ratio from the same data is shown in Figure 2. As can be seen, most of the X-rays are soft. Figure 3 shows the lightcurve from Swift-XRT data. The lightcurve has gaps because Swift is a low-earth orbit satellite, it can only take snapshot observations. The corresponding hardness ratio is shown in Figure 4. Similar characteristics, i.e high variability and predominant soft X-ray emission, are also observed.

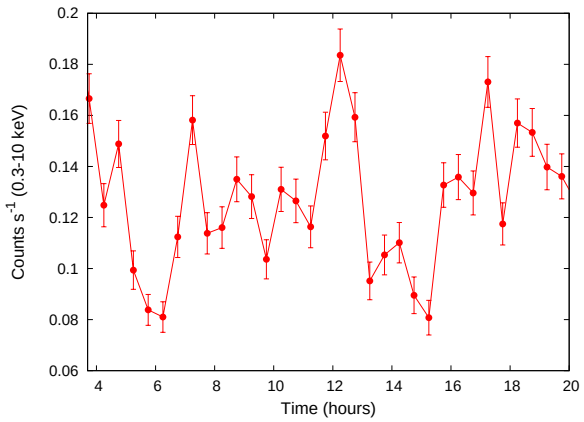

Figure 1. X-ray lightcurve from Chandra.

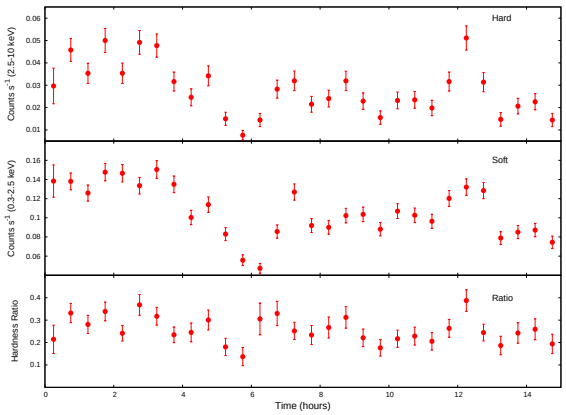

Figure 2. Hardness ratio from Chandra.

3.2. Chandra spectra

For each diffraction order and grating arm, a background subtracted spectrum was plotted and models fitted. The energy spectra are plotted in Figures 5 and 6 for HEG, and Figures 7 and 8 for MEG, for the diffraction orders m = -1 and m = +1 respectively. Each of the HEG spectra is fitted with a two-temperature vmekal model, whereas the MEG spectra are fitted with a three-temperature vmekal model. These indicate that a thermal emission process is likely. Each of the figures is characterised by a number of emission lines superimposed on the continuum emission, and most of which are in the soft X-ray band, which is the dominant contribution to

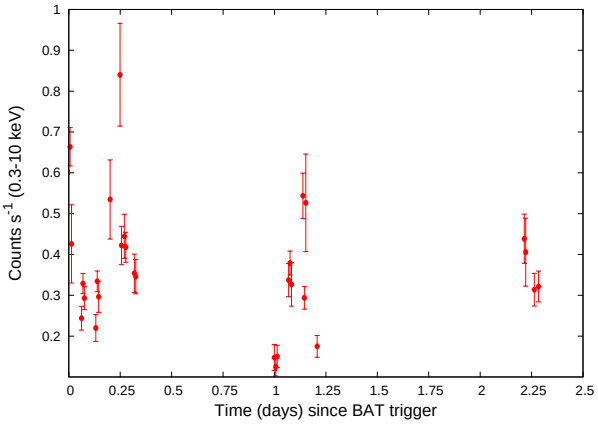

Figure 3. X-ray lightcurve from Swift data.

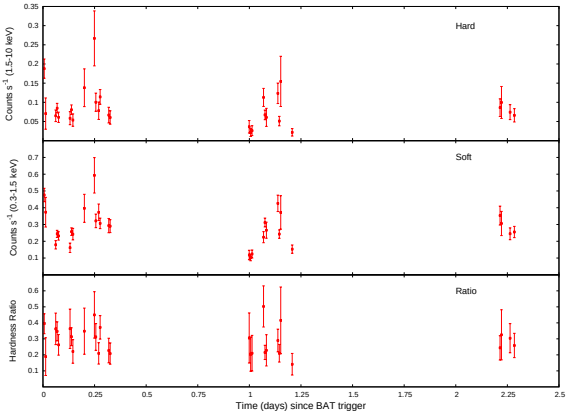

Figure 4. Hardness ratio from Swift data.

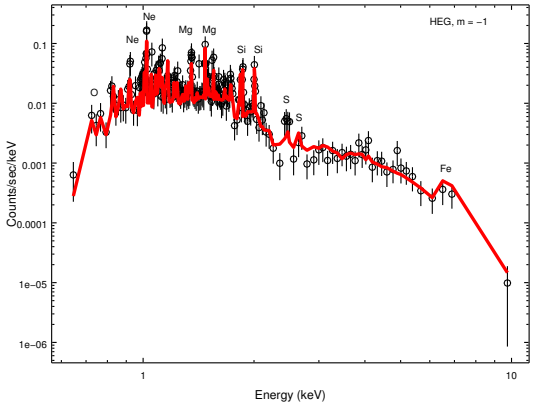

Figure 5. HEG spectrum for diffraction order m = -1 ($kT_1 \sim 0.65$, $kT_2 \sim 3.37$ keV).

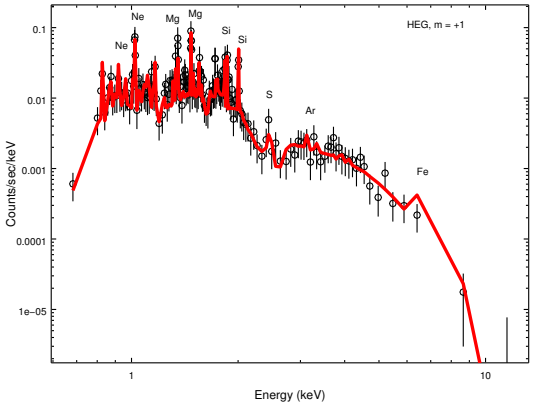

Figure 6. HEG spectrum for diffraction order m = +1 ($kT_1 \sim 0.67$, $kT_2 \sim 3.20$ keV).

the X-ray emission. The average flux of X-ray emission is $\sim 8.1{\times}10^{-12}$ erg cm^{-2} s^{-1} for HEG, and $1.0{\times}10^{-11}$ erg cm^{-2} s^{-1} for MEG respectively. For an estimated source distance of 100 pc (e.g. Welsh *et al* 1993), then it can be shown that the X-ray luminosity for each grating arm is $\sim 9.7{\times}10^{30}$ erg s^{-1} and $1.3{\times}10^{31}$ erg s^{-1} respectively. These values are similar to the X-ray luminosities reported from other observations.

3.3. Swift-XRT spectra

Figure 9 is the spectrum generated in XSPEC, and fitted with a combination of an absorbed power-law and a two-temperature vmekal emission model, suggesting that the X-ray emission has both thermal and non-thermal characteristics. In Figure 10, the unfolded models are plotted with the data, and again one can see emission line features. Hard X-ray data (kT $>$ 2 keV) are well fitted by the power-law model. The flux of soft X-rays is $\sim 6.2{\times}\ 10^{-12}$ erg cm^{-2} s^{-1}, and the corresponding hard X-rays is $4.7{\times}\ 10^{-12}$ erg cm^{-2} s^{-1}. These lead to the X-ray luminosities of $7.5{\times}10^{30}$ erg s^{-1} and $5.6{\times}10^{30}$ erg s^{-1} for soft and hard X-rays respectively, for $D \sim 100$ pc. Then, the total X-ray luminosity is $L_{\rm X} \sim 1.3{\times}10^{31}$ erg s^{-1}.

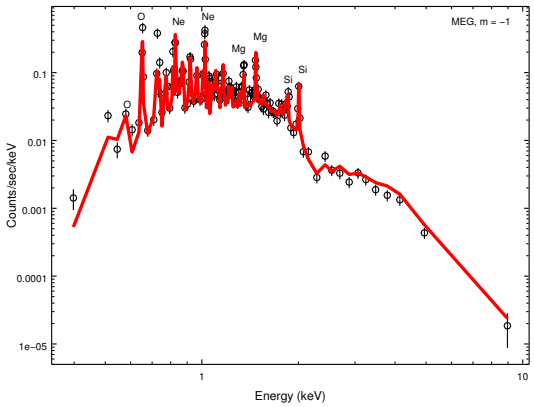

Figure 7. MEG spectrum for diffraction order m = -1 ($kT \sim 0.20$, 0.68 and 3.82 keV).

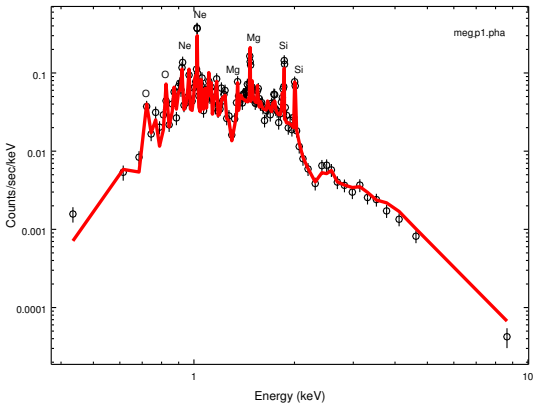

Figure 8. MEG spectrum for diffraction order $m = +1$ ($kT \sim 0.40$, 0.82 and 3.83 keV).

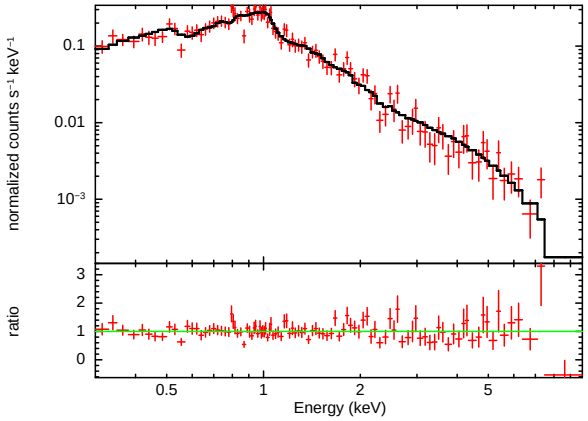

Figure 9. XRT spectrum with the best fitting models ($p \sim 2.19$, $kT \sim 0.44$, 0.96 keV).

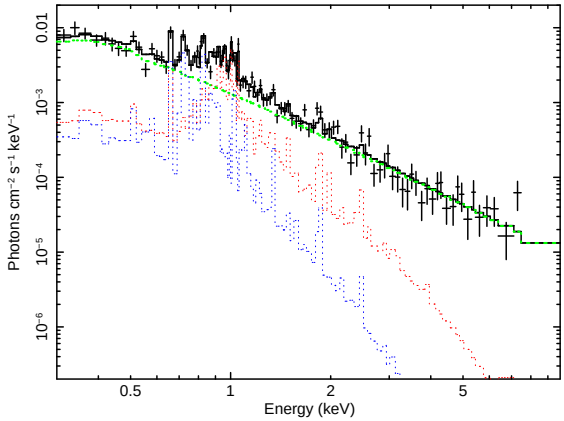

Figure 10. Unfolded models plotted with data: power-law (green), vmekal (red & blue).

4. Period analysis

Using the Swift-XRT data, we searched for periodicities in the barycenter corrected lightcurves. Epoch folding method was used, where a lightcurve is folded with large number of periods around an approximate value, and the best period found by chi squared maximization. In this case, the 33.08 s spin period of the WD and the de Jager *et al* (1994) $\dot{P} \sim 5.642 \times 10^{-14}$ s s^{-1} were used to fold the data. Figures 11 and 12 show the best periods obtained for the soft and hard X-rays. The hard X-ray emission is pulsed at a slightly higher period than the spin period of the WD.

Using the best period of 33.078060116102 s obtained in the epoch folding search for the entire X-ray data (0.3-10 keV), pulse profiles were constructed for each data set using the de Jager *et al* (1994) ephemeris. Figures 13 and 14 show the pulse profile for the soft and hard X-rays respectively. The profile for the entire X-ray energy range of the Swift data is shown in Figure 15, and Figure 16 shows the profiles for all the data sets considered. The hard X-ray data shows a shallow modulation, similar to the results reported by Terada *et al* (2008) from the analysis of Suzaku data. The average X-ray pulse profile is generally that of soft X-rays since it is the dominant component. The broad pulse profile of the hard X-rays would suggest a different emission region from the soft X-rays. This will be examined in a separate paper.

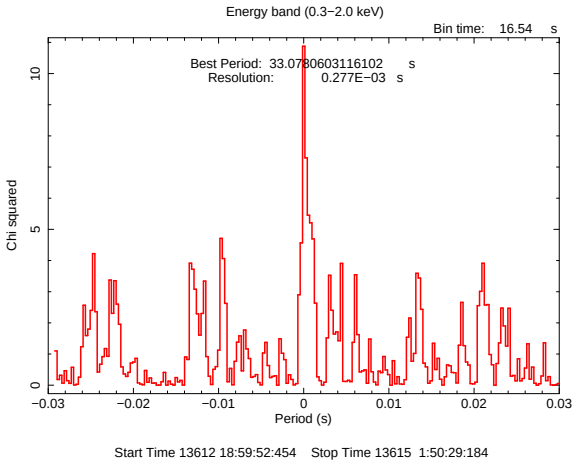

Figure 11. Best period determned for the soft rays (0.3-2 keV) is $\sim$ 33.078 s.

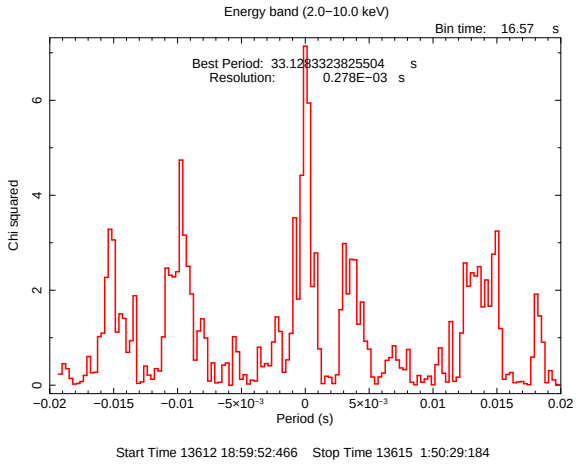

Figure 12. Best period determned for the hard X-rays (2-10 keV) is $\sim$ 33.13 s.

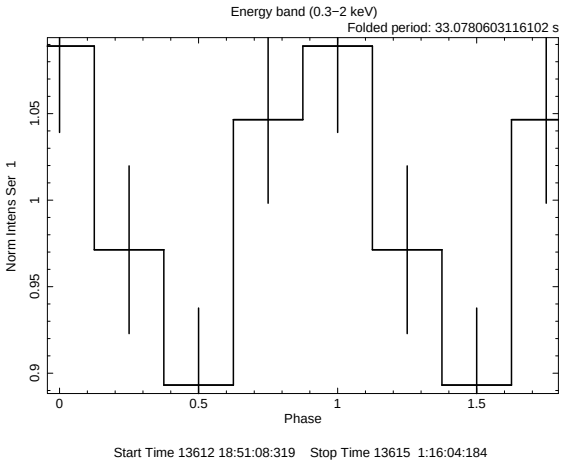

Figure 13. Folded pulse profile for the soft X-rays (0.3-2 keV).

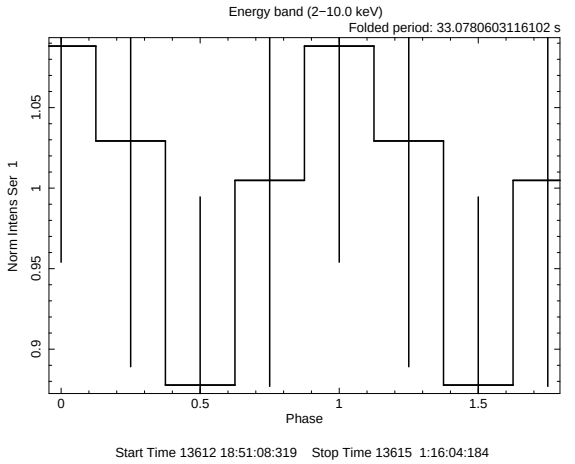

Figure 14. Folded pulse profile for the hard X-rays (2-10 keV).

5. Discussion

The lightcurves of AE Aqr showed that the source is highly variable and it exhibits periodic flares. Since AE Aqr is a non-eclipsing binary system, the variability is most likely the result of the variation in the mass accretion rate. Flares could be the result of sudden increase in the emission due to sporadic mass accretion onto the magnetosphere. Both timing and spectral analysis have revealed that most of the X-ray emission is soft. The spectra show a number of emission line features, and can be fitted with a multi-component thermal emission model. These characteristics suggest the existence of an optically thin emission region.

Using Swift-XRT data, it was shown that the hard X-ray component has a luminosity of $L_{\rm x,hard} \sim 5.6{\times}10^{30}$ erg s^{-1}. For AE Aqr, the spin-down power is $L_{\rm s-d} \sim 6{\times}10^{33}$ erg s^{-1}. Then, it can be seen that $L_{\rm x,hard} \sim 10^{-3} L_{\rm s-d}$, a relationship that has observationally been shown to hold for rotation-powered pulsars (e.g. Becker & Trümper 1997). This suggests that only a small proportion of the spin-down power is needed to power the non-thermal X-ray emission.

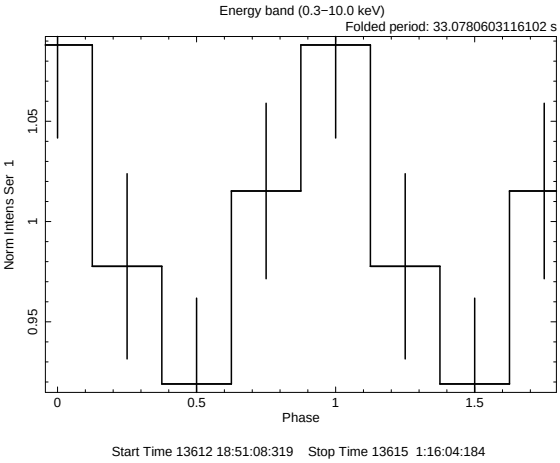

Figure 15. Folded pulse profiles for the energy range (0.3-10 keV).

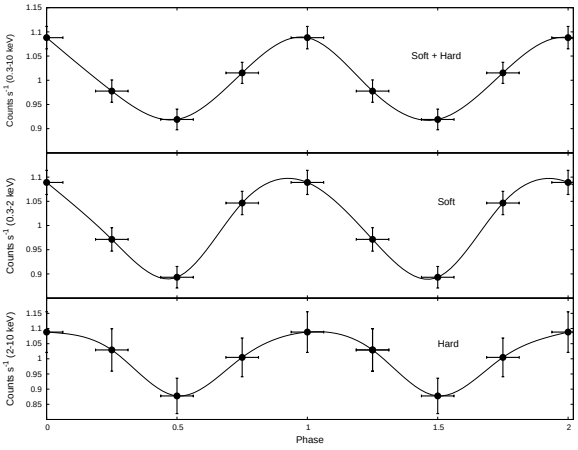

Figure 16. Folded pulse profiles for all the data sets considered.

Acknowledgments

This work made use of data supplied by the Chandra X-ray Center, and the UK Swift Science Data Centre at the University of Leicester. The research has been funded by the African Square Kilometre Array Project, and the National Research Foundation of South Africa.

References

[1] Becker W and Trümper J 1997 *Astron. Astrophys.* **326** 682
[2] Bookbinder J A and Lamb D Q 1987 *Astrophys.J* **323** 131
[3] Brissenden R J 2001 *ASP Conf. Ser.* **238** 22
[4] Burrows D N *et al* 2005 *Space Sci. Rev.* **120** 165
[5] de Jager O C 1991 *Astrophys.J* **378** 286
[6] de Jager O C, Meintjes P J, O'Donoghue D and Robinson E L 1994 *Mon. Not. R. Astron. Soc.* **267** 577
[7] Eracleous M, Horne K, Robinson E L, Zhang E, Marsh T R and Wood J H 1994 *Astrophys.J* **433** 313
[8] Evans P A *et al* 2007 *Astron. Astrophys. 469* 379
[9] Evans P A *et al* 2009 *Mon. Not. R. Astron. Soc.* **397** 1177
[10] Gehrels N *et al* 2004 *Astrophys.J* **611** 1005
[11] Itoh K, Okada S, Ishida M and Kunieda H 2006 *Astrophys.J* **639** 397
[12] Mauche C W 2006 *Mon. Not. R. Astron. Soc.* **369** 1983
[13] Meintjes P J, de Jager O C, Raubenheimer B C, Nel H I, North A R, Buckley D A H and Koen C 1994 *Astrophys.J* **434** 292
[14] Patterson J 1979 *Astrophys.J* **234** 978
[15] Patterson J, Branch D, Chincarini G and Robinson E L 1980 *Astrophys.J* **240** L133
[16] Terada Y, Ishida M, Mukai K, Dotani T, Makishima K, Naik S, Hayashi T, Okada S, Nakamura R and Enoto T 2008 *Advances in Space Research* **41** 512
[17] Welsh W F, Horne K and Gomer R 1993 *Astrophys.J* **410** L39
[18] Welsh W F, Horne K and Oke J B 1993 *Astrophys.J* **406** 229
[19] Welsh W F, Horne K and Gomer R 1995 *Mon. Not. R. Astron. Soc.* **275** 649
[20] Wynn G A, King R A and Horne K 1997 *Mon. Not. R. Astron. Soc.* **286** 436